
Hinge-Wasserstein: Mitigating Overconfidence in Regression by Classification

Ziliang Xiong¹, Abdelrahman Eldesokey², Joakim Johnander³, Bastian Wandt¹, Per-Erik Forssén¹

Computer Vision Laboratory, Department of Electrical Engineering, Linköping University¹

Visual Computing Center, KAUST²

Zenseact, Sweden³

{name.surname}@liu.se, {name.surname}@kaust.edu.sa

Abstract

Modern deep neural networks are prone to being overconfident despite their drastically improved performance. In ambiguous or even unpredictable real-world scenarios, this overconfidence can pose a major risk to the safety of applications. For regression tasks, the *regression-by-classification* approach has the potential to alleviate these ambiguities by instead predicting a discrete probability density over the desired output. However, a density estimator still tends to be overconfident when trained with the common NLL loss. To mitigate the overconfidence problem, we propose a loss function, *hinge-Wasserstein*, based on the Wasserstein Distance. This loss significantly improves the quality of both aleatoric and epistemic uncertainty, compared to previous work. We demonstrate the capabilities of the new loss on a synthetic dataset, where both types of uncertainty are controlled separately. Moreover, as a demonstration for real-world scenarios, we evaluate our approach on the benchmark dataset *Horizon Lines in the Wild*. On this benchmark, using the hinge-Wasserstein loss reduces the Area Under Sparsification Error (AUSE) for horizon parameters slope and offset, by 30.47% and 65.00%, respectively.

1 Introduction

Deep neural networks have revolutionized computer vision, producing accurate predictions on a large variety of tasks. However, for safety-critical applications, it is crucial to also obtain good uncertainty estimates. Many tasks are inherently stochastic, *e.g.*, trajectory prediction in autonomous driving or object detection in adverse weather conditions. Moreover, there is always a risk that the neural network is fed with data outside of the training distribution. These two scenarios are usually referred to as being subject to *aleatoric* and *epistemic* uncertainty, respectively¹. When such scenarios are encountered, the neural network needs to estimate and convey its uncertainty.

For regression tasks, one approach to uncertainty modeling is to directly predict the uncertainty [17, 7]. The predicted regression value is then interpreted as the mean and the predicted uncertainty as the variance of a normal distribution. Unfortunately, this formulation cannot describe probability distributions with multiple modes. Instead, non-parametric density estimation can be used, as in – so-called *regression-by-classification* – where the regression space is divided into different bins, and the task is to predict the probability of the value falling into each bin [13, 31]. This representation has the advantage of being able to capture multi-modal probability distributions. Fig. 1 shows examples of regression by classification outputs from the proposed method on the horizon line estimation task.

¹Aleatoric uncertainty is also known as *perceptual aliasing* and *partial observability* in the literature[30, 8], and epistemic uncertainty is also known as the *out-of-distribution* problem.

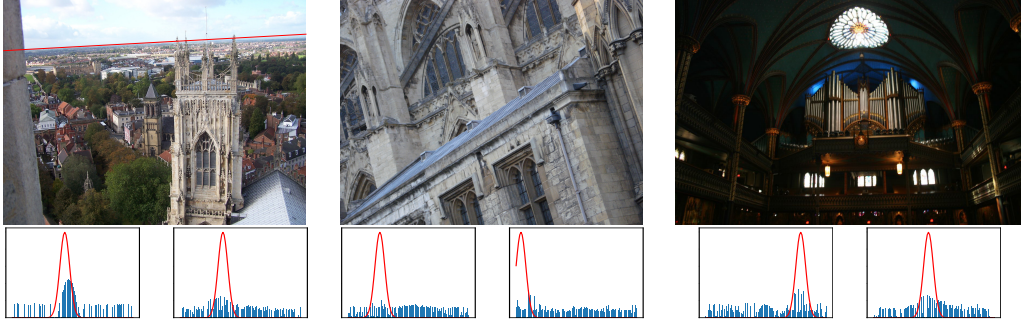


Figure 1: Horizon line detection should be framed as a probabilistic regression problem due to its inherently stochastic nature. Upper Left: Image where horizon line detection is easy (red line) and direct regression would work. Upper Middle and Right: Images where the horizon line is ambiguous. Bottom row: Plots below the images show the output probability distributions for the horizon line parameters (α, ρ) , from the proposed method. Red: ground truth; Blue: predicted density. Images are from the HLW dataset [31].

Neural networks that perform classification are typically trained by minimizing the negative log-likelihood (NLL) of the ground truth given the predicted categorical distribution. For regression-by-classification approaches, however, it has been argued that the regressed variable value should also be taken into account [13]. This can be accomplished by using a loss based on the Wasserstein distance between ground truth and predicted distributions.

The first contribution of this paper is an analysis of the uncertainty estimation capabilities of approaches based on regression-by-classification. To this end, we construct a synthetic dataset, where aleatoric and epistemic uncertainty are known and can be controlled separately. The dataset contains images of lines and the neural network is tasked with predicting the line parameters. We test aleatoric uncertainty in the form of an additional line in the image. The neural network is then unable to know which of the two lines it should report, and should convey this uncertainty in its output. Epistemic uncertainty is tested using lines with slopes outside the range encountered during training. For such cases, the neural network should also report a high uncertainty. Based on these experiments, we find that both the NLL and the plain Wasserstein losses lead to overconfident predictions.

Our second contribution is an adjustment to the Wasserstein loss, which we call *hinge-Wasserstein*. It comprises a hinge-like mechanism that, during loss computation, disregards the parts of the probability density that are below a predefined threshold. The remainders are normalized, and the Wasserstein distance is applied. This loss is more permissive with uncertain predictions. We find that this mechanism substantially improves both aleatoric and epistemic uncertainty estimates, and can be used to detect out-of-distribution samples.

Finally, we analyze the uncertainty estimates and the hinge-Wasserstein loss on a real-world computer vision dataset. We use the *Horizon Lines in the Wild* (HLW) benchmark announced in [31], which comprises an important vision task: predict the slope and offset of the horizon in an image. This problem has many applications in image metrology, prior-guided pedestrian and vehicle detection, and perspective correction in consumer photographs. Horizon lines are not always observable in a photo, depending on the camera pose, which introduces uncertainty to the problem. On this real-world benchmark, we find that both the NLL loss and the Wasserstein loss provide poor uncertainty estimates. The proposed Wasserstein loss – the hinge-Wasserstein –, however, substantially improves the uncertainty estimates, reducing the Area Under Sparsification Error (AUSE) for the slope by 30.47% and 65.00% for the offset.

2 Related Work

Regression-by-Classification: The main principle for regression-by-classification is transforming regression problems into classification. This is achieved by discretizing the continuous target variables into custom bins given some prior knowledge about the problem or automatically calculated ranges. Several classical regression approaches adopted this strategy such as Support Vector Regression (SVR), ordinal regression, and decision trees regression. In deep learning, these classical approaches were adapted to be differentiable, and thus operate in end-to-end learning frameworks [19, 24, 6].

Other approaches employed this concept to solve specific problems. Fu *et al.* [9] proposed Spacing-Increasing Discretization (SID) strategy to solve the problem of monocular depth estimation as an ordinal regression problem. Bhat *et al.* [3] proposed to use adaptive bins, and estimate the final depth values as linear combinations of these bins. A similar strategy was followed by Niu *et al.* [22] to tackle the problem of age estimation using a series of binary classification sub-problems. Workman *et al.* [31] compared regression-by-classification with direct regression on the task of horizon line detection and showed that it performs significantly better. Despite this success of regression-by-classification, one major issue is how to mitigate prediction overconfidence induced by the use of a Softmax function in classification networks [10]. To this end, we study this issue and attempt to mitigate it by introducing a better-calibrated loss function.

Uncertainty estimation with CNNs: As shown by Guo *et al.* [12], modern neural networks suffer from the problem of overconfidence, especially when they get deeper and contain more parameters. Therefore, quantifying the uncertainty of the prediction has been drawing increasing attention. The authors propose a *temperature scaling* approach to calibrate the uncertainty. The idea is to raise the output entropy while retaining the maximum of the softmax output. Other approaches to estimating uncertainty can be divided into *parametric approaches*, which are usually more task-specific; *ensemble methods* that are black-box and can be applied to most tasks; and *regression-by-classification*, which output full distributions. Parametric approaches use a hard assumption of the output distribution as an inductive bias. The neural network is designed to predict the parameters of this assumed distribution. A common inductive bias for regression tasks is a Gaussian distribution and the regressor will thus predict its mean and variance. The NLL of the parametric distribution is then used as training loss [20]. The target distribution is highly specific for a certain task. E.g., for the object detection task, Hess *et al.* [15] interprets the detector output as parameters of multi-Bernoulli (MB) and Poisson multi-Bernoulli (PMB) densities. Ensemble methods estimate uncertainty by producing a set of outputs that can be used to characterize the uncertainty. In Monte Carlo dropout [10], dropout is used during inference. By repeating the forward pass multiple times with different dropout masks, the model generates a distribution of predictions, from which the uncertainty can be estimated. A related, but more expensive method is a direct ensemble, where multiple instances of the same architecture with different random initializations and batch reshuffling are trained on the same dataset. Their predictions are then combined to obtain an estimate of uncertainty. Since this requires no modification to the model architecture, it can be combined with the parametric approach to achieve better calibration [16]. The downside with the ensemble approach is that it is relatively computationally expensive to train ensembles. Thus, it usually serves as the baseline. Regression by classification [31, 13, 8] instead outputs non-parametric distributions that can be used to characterize the uncertainty, using, *e.g.*, Shannon entropy [13] or by detecting multi-modal outputs [8]. Early papers on regression-by-classification call the technique *channel representation* [23, 8] or *population coding* [26]. We also use regression-by-classification and introduce a new loss that is more permissive of multi-modal distributions.

Horizon line estimation: There are several previous works on horizon detection, and we briefly summarize these here. Workman *et al.* [31] was the first work that proposed to use a deep convolution neural network (CNN) to directly estimate the horizon line. It also published a benchmark dataset, *Horizon Lines in the Wild* (HLW), containing real-world images with labeled horizon lines. The HLW-Net [31] has a GoogleNet [27] feature backbone, which is followed by a fully connected layer that feeds two classification heads, that predict discretized PDFs for horizon line parameters (α, ρ) . The network is trained by soft-argmax and a cross-entropy loss. Brachmann *et al.* [5] treated horizon detection as a linear regression problem by adopting neural-guided RANSAC and achieved better performance. It uses a general-purpose CNN to predict a set of 64 2D points and sampling probabilities for each output point. Then it fits a line with RANSAC. Although each point has a sampling score, it fails to transfer to the probabilistic distribution of the line. SLNet [21] is an architecture to find semantic lines and surpassed the other approaches. It comes up with line pooling layers that extract line features from convolutional feature maps. Though it has a classification head that decides if a candidate line is a semantic line, it does not address the distribution of the line. In this paper, we build upon the work of Workman *et al.* [31], given the open-source dataset and its end-to-end model architecture.

3 Method

In *regression-by-classification*, a regression variable $y \in \mathbb{R}$ is discretized into K bins. A neural network Z then predicts a conditional probability $p(y|\mathbf{x})$ given the evidence \mathbf{x} , which in our case is an image. The output of the network $\hat{p}_y = Z(x)$ in the K -probability-simplex is a vector where each element represents the probability that the regression variable y lies in a specific interval k ,

$$\hat{p}_y[k] \approx P(v_k < y < v_{k+1}|\mathbf{x}) , \quad (1)$$

where $\{v_k\}_{k=1}^{K+1}$ are the bin edges. Ensuring that \hat{p}_y is on the K -probability-simplex is most commonly achieved via the softmax function. We instead follow Häger *et al.* [13] and apply the softplus function followed by normalization, which the authors found beneficial for regression-by-classification.

The final regression prediction \hat{y} is obtained by applying some decoding function to the output vector \hat{p}_y , *i.e.*, $\hat{y} = \text{dec}(\hat{p}_y)$. The decoding function dec can be defined in different ways as explained in [8] depending on the exact representation of p_y . Here, we follow [31], and compute the decoding as the `argmax` of the output vector \hat{p}_y . In addition to decoding, it is also possible to compute an uncertainty measure with some predefined function f either given only the output vector $u = f(\hat{p}_y)$, or also including the regressed prediction $u = f(\hat{p}_y, \hat{y})$. This is discussed further in section 3.4.

3.1 Training Regression-by-Classification Networks

Training regression-by-classification networks requires defining a loss on the output vector \hat{p}_y with respect to some ground truth annotation p_y^* . Usually, only a single continuous value, y^* , is given as ground truth. This can be interpreted as the corresponding distribution being a Dirac impulse, $p_y^* = \delta_{y^*}$. A natural choice for this setting is to adopt the NLL of y^* under the predicted distribution, \hat{p}_y [31]². Kendall *et al.* [18] propose to minimize the decoding error, \hat{y} , instead, but as argued by Häger *et al.* [13], this can lead to a biased output when aleatoric uncertainty is present.

A simple way to introduce some influence of the variable value outside the single active bin in δ_{y^*} , is to define a soft peak around y^* , for instance by centering a Gaussian PDF at y^* [13]³. We adopt this approach and define the target distribution using the Gaussian PDF $g(\mu, \sigma)$ as

$$p_y^*[k] = \int_{v_k}^{v_{k+1}} g(y - y^*, \sigma) dy . \quad (2)$$

We also truncate y^* to the bin center location, to make the method more similar to the use of a single bin target used by Workman *et al.* [31].

3.2 Wasserstein Loss

The output labels in a regression-by-classification network have an inherent order, see (1). The errors caused by predicting a bin next to the correct one are thus less severe than predicting one farther away. This detail is ignored by the standard cross-entropy loss, and it has thus been argued that the Wasserstein loss is a better fit for regression-by-classification [13]. The Wasserstein loss between a predicted distribution $p(y)$ and the ground truth $q(y)$ over some variable y is defined as [29]

$$W^m(p, q) = \inf_{\gamma \in \Gamma(p, q)} \int \int |y' - y|^m \gamma(y, y') dy dy' , \quad (3)$$

where $\Gamma(p, q)$ is the set of all possible transport plans that take q to p . In the case of $m = 1$ the search over transport plans can be avoided [29, 28] as the loss simplifies to

$$W^1(p, q) = \int |P(y) - Q(y)| dy . \quad (4)$$

Here, P and Q are the CDFs of p and q respectively, *i.e.* $P(y) = \int_{-\infty}^y p(y') dy'$ and $Q(y) = \int_{-\infty}^y q(y') dy'$. In the discrete case, each PDF is represented as a set of bin values $\{p[k]\}_{k=1}^K$, with

²With some abuse of notation as \hat{p}_y is a discrete distribution.

³In [13] synthetic training data with true disparity annotations were used, including an occasional secondary disparity peak.

$\sum_k p[k] = 1$, and the loss becomes

$$W^1(p, q) = \sum_{k=1}^K |P[k] - Q[k]| = \sum_{k=1}^K |D[k]|, \text{ for } D[k] = \sum_{l=1}^k p[l] - q[l] . \quad (5)$$

Note that (5) also hints a practical way to compute this loss. In the supplementary material, we prove that this closed-form solution for 1-dimensional discrete distributions is a proper scoring rule.

3.3 Hinge-Wasserstein Loss

Most of the datasets used in computer vision are annotated with crisp ground truth, *i.e.*, instead of full conditional density annotations, only the most likely output is provided as the ground truth target to predict. When we use a loss that rewards output of only a single peak at the annotation, we effectively discourage the output to represent aleatoric uncertainty, which in turn causes overconfidence. In the extreme case, when there is no evidence to support *any* hypothesis, the output of (1) should be uniformly distributed, *i.e.* $p[k] = 1/K \quad \forall k$.⁴

An intuitive way to use crisp ground truth to learn probability density outputs is to discount the loss for all bins by a margin γ_W , and not penalize bins that are below this level. This will allow aleatoric uncertainty in the input to be represented in the output. This is similar to the hinge losses from support vector machines and to the triplet loss used in contrastive learning [25], where it only matters if the distance to a negative is larger up to a certain point. Similarly, we allow incorrect bins to be non-zero, as long as they are sufficiently below the level of the main mode.

In detail, both the predicted probability density and the Gaussian-smoothed ground truth will be discounted by the threshold, passed through a ReLU and then re-normalized to sum to one,

$$\tilde{p}[k] = \max(p[k] - \gamma_W, 0) , \quad (6)$$

$$\bar{p}[k] = \frac{\tilde{p}[k]}{\sum_k \tilde{p}[k]} . \quad (7)$$

The loss is defined by the Wasserstein distance between the two renormalized probability densities,

$$\mathcal{L}(p, q) = W^1(\bar{p}, \bar{q}) . \quad (8)$$

We call this new loss the *hinge-Wasserstein* loss. The loss removes the impact of less certain bins and penalize only bins for which a high probability has been predicted. Another way to allow for aleatoric uncertainty is to add a negative entropy term to the loss function. By minimizing the negative entropy, we maximize the entropy, which encourages uniform distribution output. The resulting loss is

$$\mathcal{L}(p, q) = W^1(p, q) - \gamma_H H(p) , \quad (9)$$

where γ_H scales the influence of the uniformity prior. The two approaches given by (8), (9) are compared experimentally in section 4.2.

3.4 Uncertainty Measure

We use *sparsification plots* [1, 16] to assess the quality of the network probability density output. This requires a scalar uncertainty value u , which is a function of the network probability density output, $\hat{p}_y = Z(\mathbf{x})$,

$$u = f(\hat{p}_y) . \quad (10)$$

The sparsification curve assesses how well the predicted uncertainty predicts the output error. The curve is generated by sorting all samples according to u in (10) and plotting the average error against the fraction of samples removed by thresholding on u . The oracle sparsification indicates the lower bound by replacing u with the absolute value of the error between the prediction and the ground truth. See Fig.3 for an example. The *area under sparsification error* (AUSE) curve [16] is defined as the area between curves from the oracle and the uncertainty measure. The AUSE measure enables a fair comparison of different methods and is the main metric for uncertainty estimation.

⁴Note that what we expect to see is the dataset prior. The bins, however, are usually chosen such that the dataset prior leads to a uniform distribution over the bins.

The standard deviation, u_σ , is a common uncertainty measure for regression problems. The main disadvantage of u_σ is that it can easily be dominated by secondary modes that are far from the dominant mode. Another choice is the Shannon entropy of \hat{p}_y , defined as in (11). Compared to standard deviation, entropy is a more robust uncertainty measure because it increases with the number of modes regardless of the mode locations,

$$u_H(\hat{p}_y) = H(\hat{p}_y) = - \sum_{k=1}^K \hat{p}_y[k] \log \hat{p}_y[k] . \quad (11)$$

One attractive property of entropy is that it is additive for independent events. Consider a set of N variables to be regressed, $\{y_i\}_{i=1}^N$. Assuming that the variables are independent, the joint entropy is

$$u_H(\hat{p}_{y_1 y_2 \dots y_N}) = \sum_{i=1}^N u_H(\hat{p}_{y_i}) . \quad (12)$$

This is an attractive property for regression tasks because we can obtain a single uncertainty value even while multiple values need to be regressed.

All the aforementioned uncertainty measures are defined in discrete bin index spaces, i.e., the distance is the difference between bin indexes. They can be also defined in the continuous parameter space, however, experiments reveal that it adds more noise to the sparsification curve and lead to high AUSE.

3.5 Application to Horizon Line Detection

Horizon line detection is an example task where both aleatoric and epistemic uncertainties are prevalent. Photos with low exposure, blurry photos, and occlusion will cause aleatoric uncertainty. Meanwhile, horizon line detection for indoor scenes is ill-posed and subject to a mix of epistemic and aleatoric uncertainty. See Fig. 1 for an example. A horizon line comprises the projection of all 3D ground-plane points at infinity into the image. This line is often parameterized as a slope and an offset (α, ρ) , which define the set of horizon pixel coordinates (x, y) as

$$(x \ y \ 1)^T (-\sin \alpha \ \cos \alpha \ -\rho) = 0, \quad (x, y) \in \Omega , \quad (13)$$

where Ω is the set of image coordinates. In order to make the horizon line representation in (13) unique, we also restrict the parameters to $\alpha \in [-\pi/2, \pi/2]$ and $\rho \in [0, \infty)$.

We base our architecture on the HLW-Net [31] which uses *regression-by-classification* to predict the horizon line. This is done by discretizing α and ρ into K bins each and using the bin index as a ground truth classification label. The $K = 100$ bins are chosen to be approximately equally likely to occur, by linearly interpolating the cumulative distribution function of the corresponding parameter over the training set. HLW-Net uses a GoogleNet [27] as the backbone feature extractor and adds two classification branches to predict the line parameters. The branches are jointly trained with classic softmax cross entropy loss and the final loss is the sum. To decode a predicted line, the strongest bin value is selected in each head, and the numeric output is chosen as the mean of the two bin edges.

4 Experiments

We analyze the performance of the new hinge-Wasserstein loss under aleatoric and epistemic uncertainty. We choose the task of horizon line detection from images as a real-world application because it showcases the different types of uncertainties in a visual and interpretable way. Experiments are performed in a controlled setting by creating a synthetic dataset (Sec. 4.1), allowing for an in-depth analysis of the proposed hinge-Wasserstein loss, as well as on the benchmark dataset *Horizon Lines in the Wild* (HLW) [31] (Sec. 4.2).

Model details: All models use *Resnet18* [14] as the backbone network, with the last layer replaced with a linear layer followed by a softplus and normalization. We compare the NLL, Wasserstein, entropy-Wasserstein, and hinge-Wasserstein losses.

4.1 Synthetic Dataset

We create a synthetic dataset to mimic the horizon line detection task, by randomly generating one or more lines that are then rendered on a background comprising Gaussian noise. This gives image-line

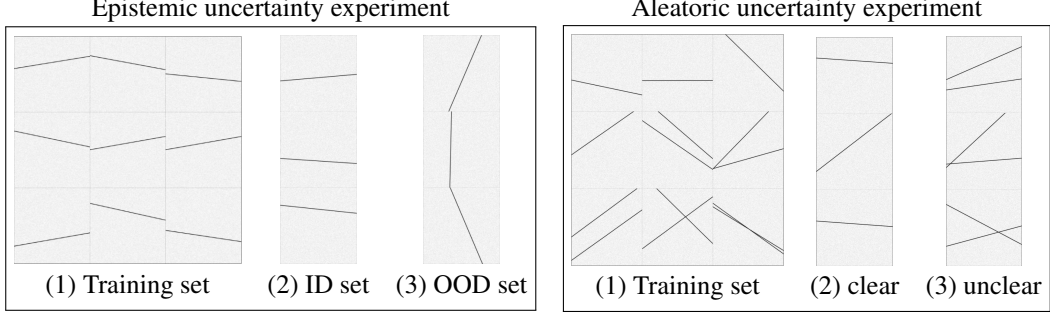


Figure 2: Examples of inputs for synthetic experiments. Left box: **Epistemic uncertainty** experiment: (1) training set, one line per image, one line as ground truth; (2) in-distribution test set; and (3) out-of-distribution test set, one line per image, but outside the training set range of values. Right box: **Aleatoric uncertainty** experiment: (1) training set, one or two lines per image, one line as ground truth; (2) test set 1, one line per image; and (3) test set 2, two lines per image.

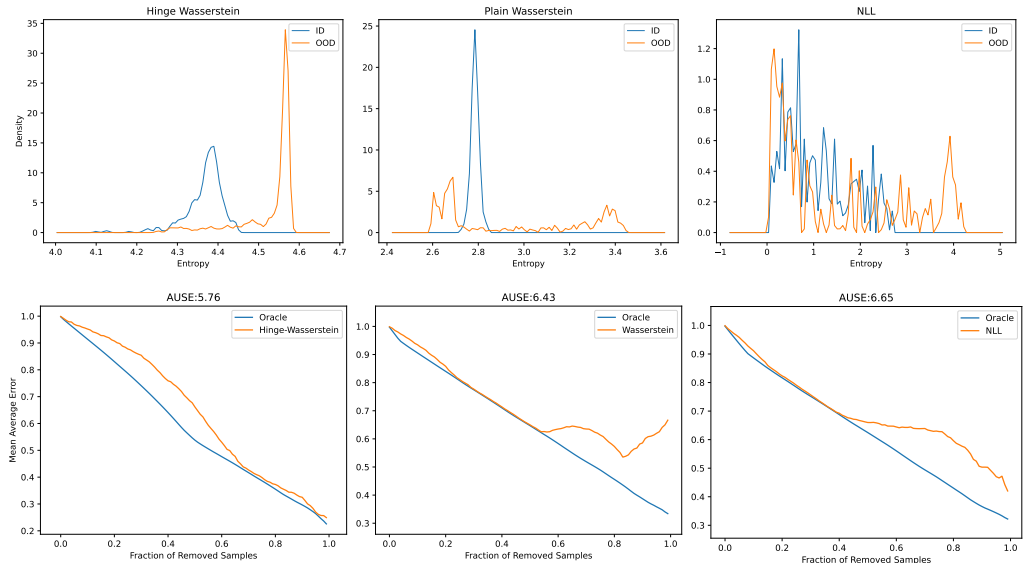


Figure 3: Top row: KDE plot of models trained with one line as the ground truth with hinge-Wasserstein $\gamma_W = 0.015$ (left), plain Wasserstein (middle), NLL (right). These plots are for the α parameter output entropy. Bottom row: sparsification plot for OOD test set of models trained with hinge-Wasserstein $\gamma_W = 0.015$, plain Wasserstein, NLL. Here, only KDE and sparsification plots for α entropy are shown because its distribution is controlled in the experiment. The KDE and sparsification plot for ρ entropy and joint entropy can be seen in the supplementary material.

pairs that can be used for supervised training. Fig. 2 shows example images for epistemic and aleatoric uncertainty. For the synthetic dataset, the usefulness of the entropy uncertainty measure on different models is assessed using *kernel density estimation* (KDE) plots [4] on the different test sets. This is done for the entropy of α , ρ , and their sum.

Epistemic Uncertainty: One of the most common causes of epistemic uncertainty is *out-of-distribution* (OOD) samples. This is simulated by the synthetic data shown on the left in Fig. 2. The training set contains 1500 samples with a single line where the slope α and the offset ρ are sampled from the uniform distributions $U_{[-\frac{\pi}{6}, \frac{\pi}{6}]}$ and $U_{[-50, 50]}$, respectively. We create two test sets: The first contains 500 *in-distribution* (ID) images, where the line is sampled from the same distribution as the training set; and the second contains the same amount of images with $\alpha \sim U_{[-\frac{\pi}{2}, -\frac{\pi}{6}] \cup [\frac{\pi}{6}, \frac{\pi}{2}]}$ and $\rho \sim U_{[-50, 50]}$. Fig. 3 shows the KDE (top) and sparsification plots (bottom) for the entropies of both test sets. The KDE of OOD samples for hinge-Wasserstein is concentrated at high entropies, while for the other losses, the OOD samples have many different entropy values, therefore, suggesting that the entropy distributions for ID and OOD examples are well-separated when using the hinge-Wasserstein loss (left) compared to the plain Wasserstein (middle) or the NLL loss (right). Conclusively, the

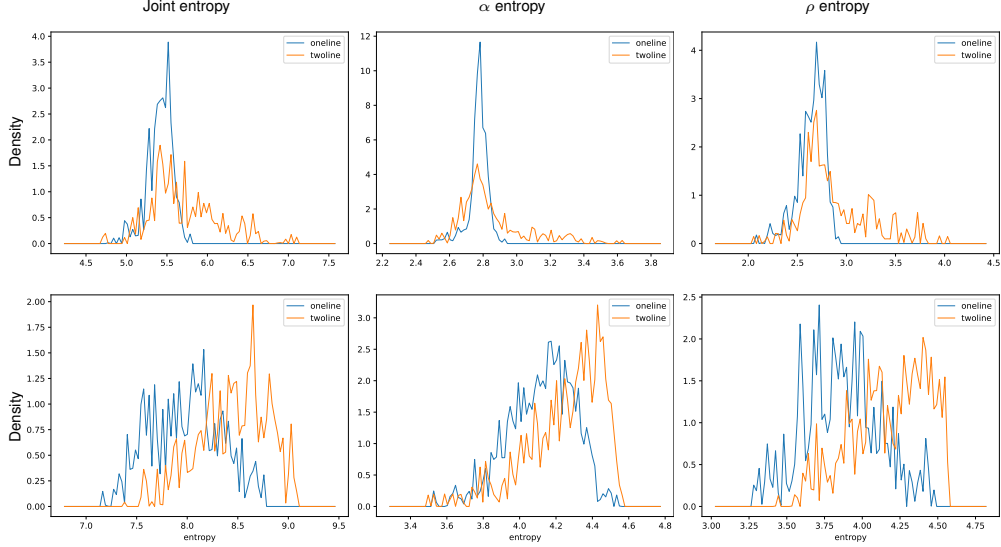


Figure 4: Epistemic uncertainty experiment. Top row: KDE plots for joint entropy, α entropy, and ρ entropy, for models trained with plain Wasserstein. Bottom row: KDE plots for joint entropy, α entropy, ρ entropy, for models trained with hinge-Wasserstein with $\gamma_W = 0.015$.

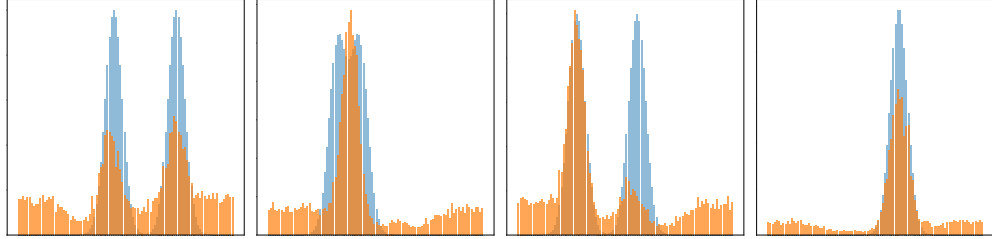


Figure 5: Density prediction for α with a model trained using hinge-Wasserstein with $\gamma_W = 0.01$, and inference on the aleatoric test sets. Blue shows ground truth, and orange shows predicted densities. (1)(3) show examples of where two output peaks overlap the ground truth; (2) shows that the model cannot distinguish two peaks if they are too close; (4) shows the model working well with unimodal ground truth. Note: Only single-line ground truth was used during training.

entropy from a network trained with the hinge-Wasserstein loss is well-suited for the detection of OOD samples. We describe a simple way to do so in the supplementary material.

Aleatoric Uncertainty: One of the most common causes of aleatoric uncertainty in horizon line detection are conflicting geometric horizon cues. To imitate such conflicting cues, we design the aleatoric uncertainty datasets shown on the right in Fig.2. The training set contains 2000 images with one line and 2000 images with two lines while still only one of these lines is labeled as the ground truth. We again create two test sets: The first contains 500 images with one line per image and the second contains 500 images with two lines per image.

Fig. 4 shows KDE plots for the one- and two-line test sets. Ideally, the mode of density on the first test set should be lower and well separated from the one on the second test set. Using the plain Wasserstein loss (top row) the network cannot distinguish images with higher aleatoric uncertainty (images with two lines) from others. However, the mode in the top row is located at the same position, and only the distributions around the mode differ. While not perfect, the hinge-Wasserstein loss improves the separation of the modes for the two distributions. Thus, we conclude that hinge-Wasserstein generates better aleatoric uncertainty estimates. To further underline this claim, Fig.5 shows qualitative examples of individual predictions. The hinge-Wasserstein captures the multimodality in the input in most cases except for the second image, the *metameric case* [8], where the modes are too close and

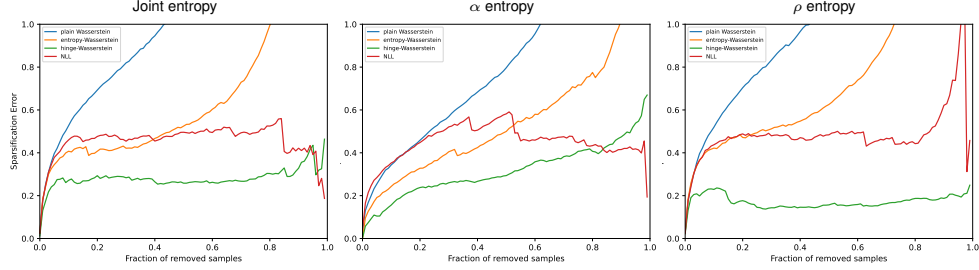


Figure 6: Sparsification error curve with joint entropy and horizon error as the oracle (left). Sparsification error curve with α entropy and absolute error as the oracle (middle). Same setting for ρ entropy (right).

Table 1: Test result on *Horizon Lines in the Wild*. For *hinge-Wasserstein* and *Entropy-Wasserstein*, $\sigma = 4$. AUC and AUSE are multiplied by 100. * indicates the value reported in the original paper.

Loss	AUC \uparrow	AUSE \downarrow	α AUSE \downarrow	ρ AUSE \downarrow
NLL Baseline Reimplementation of [31]	64.13 (64.49*)	45.20	44.30	48.00
Ours (Plain Wasserstein $\sigma = 4$)	64.29	164.30	103.30	171.30
Ours (<i>Entropy-Wasserstein</i> $\gamma_H = 0.2$)	66.46	76.80	55.50	102.80
Ours (<i>hinge-Wasserstein</i> $\gamma_W = 0.02$)	62.81	27.40	30.80	16.80

interfere. This also causes the high degree of overlap between the one- and two-line distributions in Fig.4 where the network perceives some of the two-line inputs as single-line inputs.

4.2 Real World Dataset

We compare the losses on the challenging Horizon Lines in the Wild [31] benchmark.

Evaluation Metric: The standard error metric for horizon line detection is the *horizon detection error* proposed by Barinova et al. [2]. It is calculated as the maximum vertical distance between ground truth and predicted lines in the image, normalized by the height of the image. The cumulative histogram of the horizon detection error is often used to assess the error distribution for the test set, and the area under the curve (AUC) is commonly reported as a summary statistic. Note that due to our use of an argmax decoding, there always exists a quantization error given by the bin sizes, and thus an upper bound on the AUC. This error could be reduced by using a more advanced peak decoding [8]. We leave this for future work.

Results: Table 1 shows quantitative results for different configurations of our method compared to the baseline implementation of the NLL loss [31]. Using plain Wasserstein matches the baseline in terms of the AUC metric. However, unlike in the disparity task [11] [13], it causes an even more severe overconfidence problem compared to NLL, as shown by the large AUSE score. *hinge-Wasserstein* beats the baseline by a large margin in terms of AUSE for α and ρ yet only shows a minor decrease in AUC. *Entropy-Wasserstein* can slightly improve regression performance in terms of AUC, however, its capability to handle over-confidence, as shown by the higher AUSE score, is significantly below *hinge-Wasserstein*. The sparsification error plots in Fig.6 indicate that NLL often leads to overconfident predictions for ρ as seen from the huge peak in the sparsification error curve on the right. By contrast, hinge-Wasserstein can mitigate such overconfidence.

5 Concluding Remarks

We studied different ways to improve the output uncertainty for regression-by-classification networks. Proper characterization of uncertainty is an essential component for the deployment of deep learning in safety-critical situations. As noted in [13], there is often a slight performance penalty for improved uncertainty estimation, i.e., by reducing AUSE we may degrade AUC slightly. Our experiments also show this tendency as a network trained with hinge-Wasserstein with $\gamma_W = 0.02$ has a slightly lower AUC than one trained with NLL (62.81% instead of 64.29%). However, our bare-bones system does

not exploit all techniques from classification-by-regression, e.g., more sophisticated mode decoding [8] or better placement of the target distributions around the ground truth.

More importantly, we demonstrated that it is indeed possible to mitigate the overconfidence problem in a real computer vision application, namely horizon line detection in the wild [31]. Training with the proposed hinge-Wasserstein loss improves the AUSE from 0.45 (for NLL) or 1.64 (for plain Wasserstein) to 0.27 for the proposed hinge-Wasserstein loss. One future direction would be to try the proposed loss on other regression problems.

References

- [1] Oisin Mac Aodha, Ahmad Humayun, Marc Pollefeys, and Gabriel J. Brostow. Learning a confidence measure for optical flow. *IEEE Transactions on Pattern Recognition and Machine Intelligence (TPAMI)*, 35:1107–1120, May 2013.
- [2] Olga Barinova, Victor Lempitsky, Elena Tretiak, and Pushmeet Kohli. Geometric image parsing in man-made environments. In *Computer Vision–ECCV 2010: 11th European Conference on Computer Vision, Heraklion, Crete, Greece, September 5–11, 2010, Proceedings, Part II* 11, pages 57–70. Springer, 2010.
- [3] Shariq Farooq Bhat, Ibraheem Alhashim, and Peter Wonka. Adabins: Depth estimation using adaptive bins. In *Proceedings of the IEEE/CVF Conference on Computer Vision and Pattern Recognition (CVPR)*, pages 4009–4018, June 2021.
- [4] Christopher M Bishop. *Pattern recognition and machine learning*, volume 4. Springer, 2006.
- [5] Eric Brachmann and Carsten Rother. Neural-guided RANSAC: Learning where to sample model hypotheses. In *Proceedings of the IEEE/CVF International Conference on Computer Vision*, pages 4322–4331, 2019.
- [6] Jianlin Cheng, Zheng Wang, and Gianluca Pollastri. A neural network approach to ordinal regression. In *2008 IEEE international joint conference on neural networks (IEEE world congress on computational intelligence)*, pages 1279–1284. IEEE, 2008.
- [7] Abdelrahman Eldesokey, Michael Felsberg, Karl Holmquist, and Michael Persson. Uncertainty-aware CNNs for depth completion: Uncertainty from beginning to end. In *Proceedings of the IEEE/CVF Conference on Computer Vision and Pattern Recognition*, pages 12014–12023, 2020.
- [8] Per-Erik Forssén, Björn Johansson, and Gösta Granlund. Channel associative networks for multiple valued mappings. In *2nd International Cognitive Vision Workshop*, pages 4–11, Graz, Austria, May 2006.
- [9] Huan Fu, Mingming Gong, Chaohui Wang, Kayhan Batmanghelich, and Dacheng Tao. Deep ordinal regression network for monocular depth estimation. In *Proceedings of the IEEE conference on computer vision and pattern recognition*, pages 2002–2011, 2018.
- [10] Yarin Gal and Zoubin Ghahramani. Dropout as a bayesian approximation: Representing model uncertainty in deep learning. In *International Conference on Machine Learning*, pages 1050–1059. PMLR, 2016.
- [11] Divyansh Garg, Yan Wang, Bharath Hariharan, Mark Campbell, Kilian Q. Weinberger, and Wei-Lun Chao. Wasserstein distances for stereo disparity estimation. In *NeurIPS*, 2020.
- [12] Chuan Guo, Geoff Pleiss, Yu Sun, and Kilian Q Weinberger. On calibration of modern neural networks. In *International conference on machine learning*, pages 1321–1330. PMLR, 2017.
- [13] Gustav Häger, Mikael Persson, and Michael Felsberg. Predicting disparity distributions. In *IEEE International Conference on Robotics and Automation (ICRA’21)*, pages 4363–4369, 2021.
- [14] Kaiming He, Xiangyu Zhang, Shaoqing Ren, and Jian Sun. Deep residual learning for image recognition. In *IEEE Conference on Computer Vision and Pattern Recognition*, pages 770–778, 2016.
- [15] Georg Hess, Christoffer Petersson, and Lennart Svensson. Object detection as probabilistic set prediction. In *17th European Conference on Computer Vision (ECCV)*, pages 550–566. Springer, 2022.
- [16] Eddy Ilg, Ozgun Cicek, Silvio Galesso, Aaron Klein, Osama Makansi, Frank Hutter, and Thomas Brox. Uncertainty estimates and multi-hypotheses networks for optical flow. In *Proceedings of the European Conference on Computer Vision (ECCV)*, pages 652–667, 2018.
- [17] Alex Kendall and Yarin Gal. What uncertainties do we need in bayesian deep learning for computer vision? *Advances in neural information processing systems*, 30, 2017.
- [18] Alex Kendall, Hayk Martirosyan, Saumitro Dasgupta, Peter Henry, Ryan, Kennedy Abraham Bachrach, and Adam Bry. End-to-end learning of geometry and context for deep stereo regression. In *International Conference on Computer Vision (ICCV)*, pages 66–75, 2017.
- [19] Peter Kontschieder, Madalina Fiterau, Antonio Criminisi, and Samuel Rota Bulo. Deep neural decision forests. In *Proceedings of the IEEE international conference on computer vision*, pages 1467–1475, 2015.
- [20] Balaji Lakshminarayanan, Alexander Pritzel, and Charles Blundell. Simple and scalable predictive uncertainty estimation using deep ensembles. *Advances in neural information processing systems*, 30, 2017.
- [21] Jun-Tae Lee, Han-Ul Kim, Chul Lee, and Chang-Su Kim. Semantic line detection and its applications. In *Proceedings of the IEEE International Conference on Computer Vision*, pages 3229–3237, 2017.

- [22] Zhenxing Niu, Mo Zhou, Le Wang, Xinbo Gao, and Gang Hua. Ordinal regression with multiple output cnn for age estimation. In *Proceedings of the IEEE conference on computer vision and pattern recognition*, pages 4920–4928, 2016.
- [23] K. Nordberg, G. H. Granlund, and H. Knutsson. Representation and learning of invariance. In *Proceedings of IEEE International Conference on Image Processing*, pages 585–589, 1994.
- [24] Nicolas Papernot and Patrick McDaniel. Deep k-nearest neighbors: Towards confident, interpretable and robust deep learning. *ArXiv*, abs/1803.04765, 2018.
- [25] Florian Schroff, Dmitry Kalenichenko, and James Philbin. Facenet: A unified embedding for face recognition and clustering. In *Proceedings of the IEEE Conference on Computer Vision and Pattern Recognition (CVPR)*, pages 815–823, June 2015.
- [26] Herman P. Snippe. Parameter extraction from population codes: A critical assessment. *Neural Computation*, 8:511–529, 1996.
- [27] Christian Szegedy, Wei Liu, Yangqing Jia, Pierre Sermanet, Scott Reed, Dragomir Anguelov, Dumitru Erhan, Vincent Vanhoucke, and Andrew Rabinovich. Going deeper with convolutions. In *Proceedings of the IEEE conference on computer vision and pattern recognition*, pages 1–9, 2015.
- [28] Thordis L. Thorarinsdottir, Tilmann Gneiting, and Nadine Gissibl. Using proper divergence functions to evaluate climate models. *SIAM/ASA Journal on Uncertainty Quantification*, 1(1), 2013.
- [29] M. Thorpe. Introduction to optimal transport. Lecture Notes, 2018.
- [30] Steven D. Whitehead and Dana H. Ballard. Learning to perceive and act by trial and error. *Machine Learning*, 7:45–83, 1991.
- [31] Scott Workman, Menghua Zhai, and Nathan Jacobs. Horizon lines in the wild. In *British Machine Vision Conference (BMVC)*, pages 20.1–20.12, 2016. Acceptance rate: 39.4%.